Acta Neuropathol (1998) 95 : 395–406 © Springer-Verlag 1998

REGULAR PAPER

Y. Grignon · C. Duyckaerts · M. Bennecib · J.-J. Hauw

Cytoarchitectonic alterations in the supramarginal gyrus of late onset Alzheimer's disease

Received: 24 April 1997 / Revised, accepted: 3 October 1997

Abstract The intellectual status of 28 women of over 75 years of age had been prospectively assessed by the Blessed test score. It ranged from nearly normal to deeply altered by dementia. After autopsy, the supramarginal gyrus was marked at the surface of the brain. Sections, 1 cm thick, were cut with a specially devised macrotome. The volume of the parietal lobe was measured by a point counting method, using Cavalieri principle. A sample from the supramarginal gyrus was taken from the previously marked area and the shrinkage due to the histological procedures was measured (it averaged 12%). More than 500 nucleolated neuronal profiles per case were mapped with a semi-automatic system. Density maps of the neuronal profiles were drawn and mean density was calculated using Dirichlet tessellation. The thickness of the cortical ribbon was standardized on the maps. The density of the neurons per unit volume was calculated, taking into account the section thickness measured for each sample with a length gauge fastened to the Z axis of the microscope. Statistical correlations were sought between the mean and laminar densities of the neurons on one hand, and Blessed test score, the densities of neurofibrillary tangles (NFT) and of senile plaques profiles, on the other hand. Finally, the total number of neurons present in the parietal lobe was estimated in each case. Neuronal loss appeared to be linked with the density of the NFT ($r = –0.52$; $P < 0.004$). The correlation was mainly due to a severe drop in neuronal number observed in the cases with more than 5 NFT/mm^2. An average difference of 98×10^6 neurons per parietal lobe was found between the cases with less than 5 NFT/mm^2 and those with more. The neuronal loss predominated in layers II and III (upper part). A multivariate analysis showed that the intellectual status was better correlated with the density of the tangles than with the neuronal loss.

Y. Grignon · C. Duyckaerts (✉) · M. Bennecib · J.-J. Hauw
Laboratoire de Neuropathologie R. Escourolle, INSERM U 360,
Hôpital de La Salpêtrière, 47, Boulevard de l'Hôpital,
F-75651 Paris Cedex 13, France
Tel.: 33-1-42161891; Fax: 33-1-44239828;
e-mail: charles.duyckaerts@psl.ap-hop-paris.fr

Key words Alzheimer's disease · Neuronal loss · Neurofibrillary tangle · Morphometry

Introduction

The occurrence, severity and significance of neuronal loss in the course of Alzheimer's disease (AD) have been debated: it has been said to involve middle-sized and large pyramidal neurons [45] but even the presence of a global neuronal loss has been questioned [42]. Controversies appear to be the consequence of numerous methodological difficulties [7]. Inter-individual variability of the counts is greater than usually thought and limits the precision of the estimate in a given population sample [24]. Gross atrophy, observed in AD, modifies the relationship between the density in a sample and the 'true' neuronal number: when the same number of neurons is 'diluted' in a smaller (because atrophic) volume of cortex, their numerical density increases and this may hide the neuronal loss as seen on histological sections. On the other hand, the microscopical examination involves sectioned neurons (so-called 'neuronal profiles') which are biased images of three-dimensional (3D) neurons. A decrease in the density of neuronal profiles may be due to either a decrease in the number of neurons per unit volume or the atrophy of the neuronal cell bodies [1, 4] which lowers the probability of the shrunken neurons being present in the microscopical section and gives rise to an apparent neuronal loss (pseudo-loss [16]). The technical procedures used to prepare a section for microscopy include passages in organic solvents which can cause an uncontrolled shrinkage of the samples. This shrinkage varies with age [27] and could also be modified by the pathological condition. Finally, the density of changes such as neurofibrillary tangles (NFT) and senile plaques (SP) is highly heterogeneous in the hippocampus and isocortex [2]. The degree of the neuronal loss itself also probably varies with the cytoarchitectonic areas [5–8, 40, 45]: the loss appears to be severe in the entorhinal cortex [22] and in the CA1 sector of the hippocampus [50], but is probably also noticeable in some areas of the isocortex [23, 32].

To evaluate the order of magnitude of the neuronal loss, its laminar distribution and its main correlates, we deliberately chose a well-defined cytoarchitectonic area (area 40) that was sampled in an uniform and controlled way. The position of ~ 500 neurons was mapped in each case (except in the most advanced one where the density was too low to permit the mapping of a straight portion of the cortical ribbon). Care was taken to control the variables which are involved in the final computation of the number of neurons: we measured the volume of the parietal lobe, assessed the shrinkage of the blocks, and estimated the section thickness with a "microcator" [25]. To analyze the maps, we reasoned that we had to evaluate the density of neuronal profiles at a local scale. We considered that the smallest possible scale was each individual profile. The density of a given profile was found to be solely determined by its neighbors: when they were close, the numerical density was high. This led to a "tessellation" of the plane of the map in as many small areas as there were neuronal profiles. The free area around each profile was calculated, according to a method that has already been developed in this laboratory [19].

Cases and methods

Cases

The cases belonged to a prospective study, involving all the patients admitted to a geriatric ward of a long-stay hospital (Charles Foix Longitudinal Study). These were all women of over 75 years of age (range: 75–99 years; mean: 89 years). Patients were excluded when a cause of dementia other than AD was diagnosed (e.g., stroke, Parkinson's disease, alcoholism) or when sensory deficits (blindness, deafness) precluded the testing. All the patients who accepted to enter the study were tested by the Blessed test score (BTS). Brains from 31 patients were investigated in this study. Of these brains 2 were excluded post-mortem because of ischemic lesions. One randomly chosen hemisphere was formalin fixed and neuropathologically assessed. Several sets of data are available on this cohort [10–15, 20, 29, 30].

Volume estimates

The lobes were colored before sectioning, so that they could be recognized on sections [12]. The gyrus located behind the inferior part of the postcentral gyrus and limited by the postcentral and the intraparietal sulci was identified as 'supramarginal' and labeled with India ink before cutting. Systematic 1-cm-thick coronal sections were then cut and photographed alongside a ruler. The photographic slides were examined on a video screen, where a grid of equally spaced points was drawn. Each point was surrounded by a free space of 0.25 cm^2. The number of points falling in the cortex was counted manually. The volume was evaluated by summing the surface times the mean thickness of the section, a method referred to as Cavalieri principle [24].

Sampling and histological exclusion

The supramarginal gyrus, identified and labeled before brain cutting, was sampled in such a way that at least part of the section included some cortical ribbon cut perpendicularly to its pial surface.

In one case (case 2722), ischemic cell changes were seen in the neurons of the supramarginal gyrus. Shrinkage of the neuronal profiles precluded the recognition of nucleoli. This sample was discarded from the series.

Evaluation of the shrinkage and of the thickness of the sections

The sample length and its width were measured before embedding, with a caliper square, for 25 cases (in 3 cases the data were lacking or incomplete). The blocks were embedded in paraffin, sectioned at a nominal thickness of 8 μm and stained with Harris hematoxylin. The length and the width of the sample were then assessed again and a shrinkage factor [(measurement before embedding-measurement after embedding)/measurement before embedding] was calculated. To measure the section thickness, the microscopical sections were examined at high magnification with a × 100 oil immersion lens (numerical aperture 1.25; this objective has a maximum Z resolution, expressed as full-width half maximum of 360 nm according to the Kino approximation [35]). The image was set into focus and a linear transducer Heidenhain (Digitaler Messtaster MT 12) fastened to the Z axis of the moving stage of the microscope set at zero. The moving stage was gradually moved with the micrometer screw until the image went out of focus. The distance covered by the moving stage estimated by the linear transducer (by steps of 0.5 μm) was taken as the estimate of the section thickness [43].

Estimates of lesions density

Data concerning the density of Aβ deposits (using a monoclonal antibody against Aβ protein residues 10–28, obtained from Dako, Glostrup, Denmark) and of mean density of tau-positive tangles (polyclonal; Dako) have already been published [10, 11, 13, 14].

Data acquisition

The maps were collected with the following apparatus, furnished by Biocom (software Histo): a video camera, plugged into the phototube of a microscope, transmitted the microscopical image to a video screen. Linear transducers, fastened to the moving stage of the microscope, recorded its X and Y position and fed them into a PC computer. The borders of the sample and of the regions of interest were drawn manually. The neuronal profiles were marked, using a mouse, on the video screen. These neuronal profiles remained labeled on the video screen to avoid being counted twice. At least 500 neuronal profiles were mapped for each case, except for the most severely affected one, where the density of the profiles had dropped to such a low value that only 270 neurons could be collected in a straight portion of the cortical ribbon. The mean coefficient of error of profile density obtained with that sample was 5.2%.

The criterion used to classify a profile as neuronal was the presence of a nucleolus. We measured the size of the nucleoli in a sample of 50 nucleolar profiles in the most severely affected cases (10 profiles/sample in 5 different cases) and of 50 nucleolar profiles in the least-affected ones (10 profiles/sample in 5 other cases) by direct measurement on the video screen using a × 100 lens [numerical aperture 1.25; nominal resolving power at wavelength (λ) 550 nm = 0.22 μm; however, with the condenser that was used without immersion oil and an aperture of 0.9, the resolving power was not as good and was estimated to be 0.44 μm at the worst, i.e., λ/numerical aperture]. The mean coefficient of error in the estimation of the diameter of the nucleolar profile was found acceptable with these samples (7.1% for the 5 most affected cases and 7.8% for the least affected ones). To extrapolate from the diameter of the profile to the diameter of the nucleolus in 3D, the correction factor $4/\pi$ was used [49]. The nucleolar volume was calculated according to the formula $(\pi/6) \times D^3$ (where D is the corrected diameter).

Data analysis

Coordinates of the region borders and of the neuronal profiles were stored in a file at the end of the acquisition step. These coordinates were used to analyze the data with a specially devised program developed in this laboratory (Vorcel: this program is available on request from C.D.). The following steps were used.

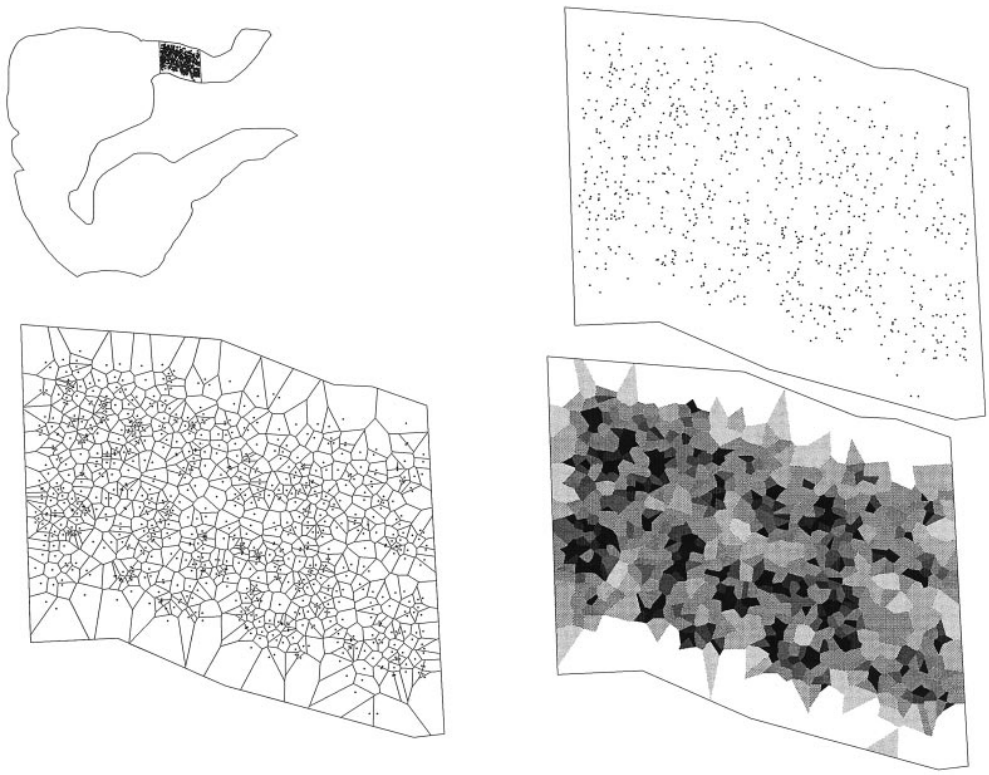

Fig. 1 Method used to draw a density map of the neuronal profiles. Neuronal profiles (nucleolated cells) were mapped in the supramarginal gyrus. The sample contained at least 500 profiles (*upper left panel*). The area where the neuronal profiles had been drawn was isolated (*upper right panel*). Around each point (corresponding to a neuronal profile) a polygon was drawn, using a specially devised program (Vorcel). Each side of a given polygon is at mid-distance between two profiles (*lower left panel*). The polygons were then colored according to their surface area: the largest ones were left white; the smallest ones were filled in black (*lower right panel*)

Tessellation

The region was divided into small polygonal areas limited by borders located at mid-distance between two neighboring neuronal profiles. Each polygon contained only one point (i.e., one neuronal profile). The polygons covered the entire area of the region without overlaps or interstices, i.e., realized a tessellation of the plane. The algorithm used to obtain this tessellation was derived from [19] and was applicable to non-convex contours (Fig. 1). The area of each individual polygon was inversely proportional to the numerical density of the profiles [19]. When the density was high, the profiles were close to each other and the polygons were small. Assigning a color to a range of areas allowed a 'density map' of the neurons to be drawn.

Evaluation of numerical mean density of neuronal profiles

The mean density of neuronal profiles and its confidence interval were computed as follows. The areas of the polygons were calculated and averaged, and the standard error, i.e., standard deviation/square root (number of neurons), of the mean polygon area was calculated. Two standard errors were added to and subtracted from the mean polygon area: 1/mean polygon area was taken as the mean density of the neurons, with 95% confidence interval, 1/(mean polygon area + 2 standard errors) and 1/(mean polygon area – 2 standard errors).

Standardization of the cortical thickness and estimation of neuronal density at various layers

Atrophy of the cortical ribbon decreases both its length [12] and its thickness [38–40]. The decrease in cortical length can only be evaluated macroscopically. The decrease in cortical thickness (i.e., the decrease in the distance between the pial surface and the white matter) is readily apparent on the sections microscopically and can be directly measured. As the space in which the neuronal profiles are distributed shrinks, the neuronal profiles density increases. This increase masks the loss. To avoid this 'masking by atrophy', the cortical thickness was standardized at 3000 μm by changing the magnification at which the sample was viewed to have it fit a window of 3000 μm in height.

Evaluation of the density of the neuronal profiles in increasing cortical depths

The cortical ribbon was divided into ten levels from the pial surface to the white matter, the pial surface corresponding to 0% and the white matter to 100% of the cortical depth. The numerical density of the neuronal profiles was measured, as described above, in each level.

Evaluation of the neuronal density per unit volume and of the total number of neurons in the parietal lobe

The shrinkage of a sample induced an overestimation of the neuronal density. The density values were corrected accordingly.

To estimate the neuronal density per unit volume (Nv) was calculated as described by Abercrombie [1]: $Nv = Na/(t+d)$, where Na = number of neuronal profiles per unit surface; t = thickness of the paraffin section (measured for each slide); d = mean nucleolar diameter.

It has been shown that the profile densities assessed by the tessellation could be similarly corrected to obtain values of volume densities, true on average [19].

The total number of neurons in the parietal lobe was taken as the product of their density (Nv without standardization of the cortical thickness) and the volume of the parietal lobe.

Results

Raw and standardized values of the density of neuronal profiles

The data for the raw density of neuronal profiles per mm^2 did not correlate with NFT density ($r = –0.312$), SP den-

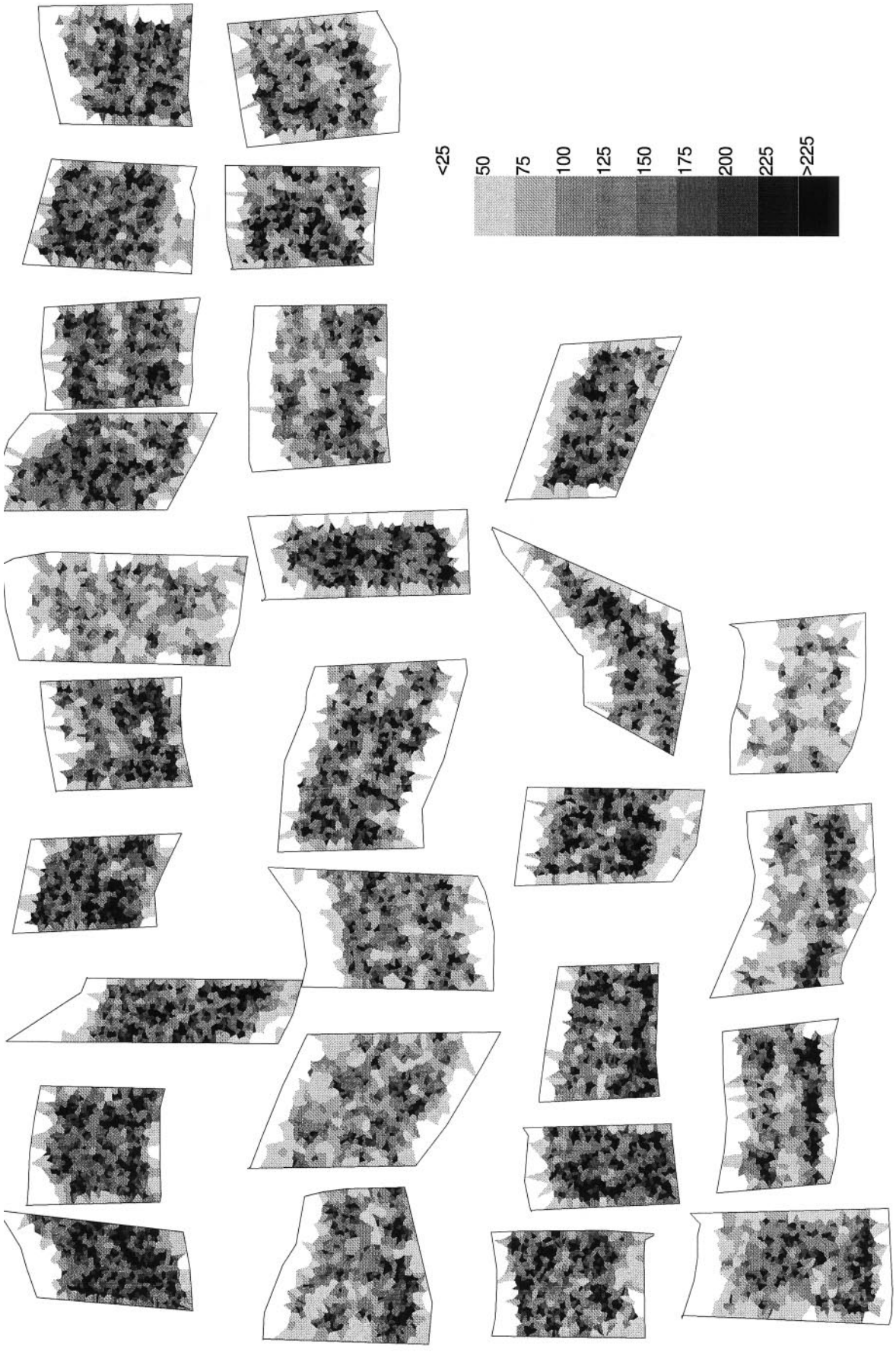

Fig. 2 Raw density maps. Each map is a sample from the supramarginal gyrus of a different case. The cases have been ranked from *left* to *right* and from *top* to *bottom* according to their density in NFT. When the density of NFT was 0, the cases have been ranked according to their intellectual status (BTS). The most advanced cases are in the *lower right corner*. Densities given on the gray scale are in number of neuronal profiles per mm^2 (*NFT* neurofibrillary tangles, *BTS* Blessed test score)

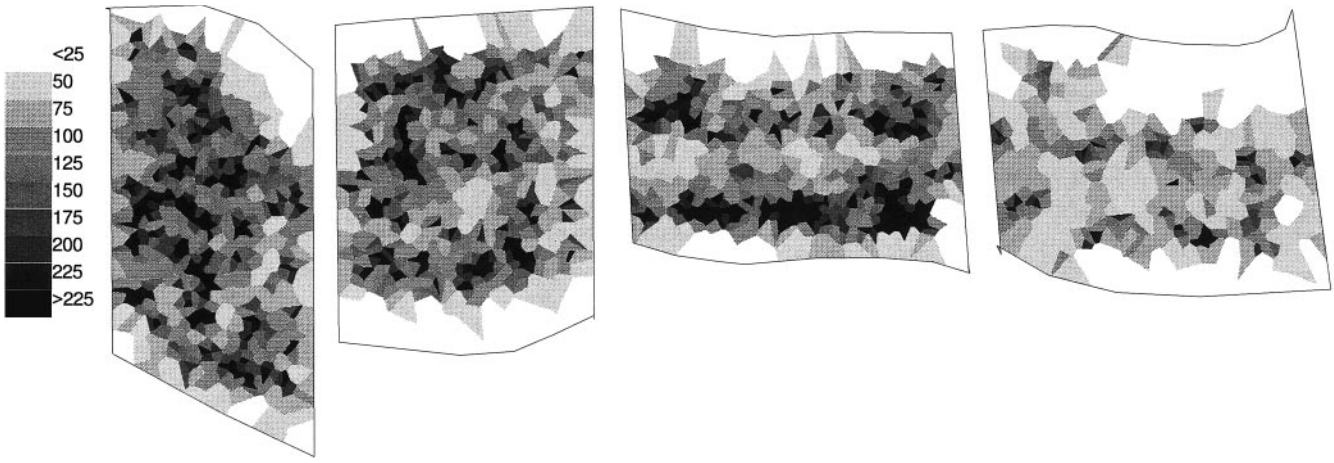

Fig. 3 Atrophy of the cortical ribbon. Four samples from the supramarginal gyrus (from *left* to *right*): a case, aged 90 years, with no NFT, BTS = 25; a case (aged 88 years) with a density of NFT of 2.5 /mm^2, BTS = 8; a case (aged 75 years) with a density of NFT of 19.5/mm^2, BTS = 2; on the *right*, a case (aged 75) with a density of NFT of 28.4/mm^2 (BTS = 0). These four views illustrate the atrophy of the cortical ribbon, inducing a decrease in cortical thickness, masking the neuronal loss. The drop in neuronal density was visible only in the most advanced case (on the *right*). Densities are in number of profiles per mm^2

sity (r = 0.06) or the BTS (r = 0.18). The density maps revealed that there was no localized drop in the density of the neuronal profiles in most of the maps (Fig. 2). The thickness of the cortical ribbon was 2690 μm on average (± a standard error of 101 μm) and varied from 1827 to 3973 μm. It did not correlate with either the BTS (r = 0.36; P > 0.05) or SP density (r = 0.212; P > 0.05), but did correlate with the mean density of NFT (r = 0.409; P = 0.028). This result indicated that a shrinkage, proportional to the density of NFT, had occurred in the course of the disease, as illustrated in Fig. 3. After the thickness of the cortical ribbon had been standardized at 3000 μm (Fig. 4), correlations were found significant between the mean density of neuronal profiles, the BTS (r = 0.39; P < 0.04) and the density of NFT (r = –0.51; P < 0.006). We then wondered whether these significant correlations were not a spurious effect of the standardization, which in effect divided the neuronal density of each sample by the thickness of the cortical ribbon, itself correlated with the density of NFT. To test this, we used a multivariate analysis with the raw density of the neuronal profiles as the dependent variable, and the thickness of the cortical ribbon and the mean density of NFT as the independent variables. The correlation was significant (r = 0.535; P < 0.02). The coefficients of the regression were as follows: density of the neuronal profiles = 153.389–1.349 × NFT/mm^2 –0.017 × thickness of the cortex; showing that the neuronal density tended to decrease with the increasing in NFT density, but that it was compensated by a shrinkage of the cortex. According to this equation, the shrinkage of the cortical thickness from 3000 to 2000 μm (with constant NFT density) would, for instance, induce an increase in expected density of neuronal profiles from 102.389 neuronal profiles/mm^2 (153.389–0.017 × 3000) to 119.389 neuronal profiles/mm^2 (153.389–0.017 × 2000). In the same way, when the neuronal density remains constant, an increase of one point in the density of NFT (expressed in n/mm^2) causes an atrophy of 0.017/1.349 of the cortical thickness, i.e., 1.3%.

Influence of the section thickness

We then asked whether the thickness of the section (of nominal thickness 8 μm) was variable, and if so, how it was related to the density of lesions. The average section thickness (± SEM) was 7.33 ± 0.14 μm (minimum 5.9 μm, maximum 8.7 μm). It varied significantly from one sample to the next. As expected, the measured section thickness of one given sample was correlated with the density of neuronal profiles per mm^2 (thick sections containing obviously more profiles than thin ones). Regression analysis showed that the number of profiles per mm^2 was 13.7 × section thickness (r = 0.979; P < 0.0001 when the regression curve was constrained to go through the point of coordinates X = 0, Y = 0, i.e., thickness = 0, density = 0): a tissue block of 1 mm^2 in area and 1 μm in thickness included on average 13.7 neuronal profiles.

To test the possibility that the section thickness was influenced by the pathology, correlations between the density of the alterations and the estimated section thickness were sought. The sections in this series of samples tended to be thicker when the NFT were numerous but this failed to reach significance (r = 0.364; P = 0.568) and did not influence the correlations to a significant extent.

Influence of the section shrinkage

Mean shrinkage for the microscopic specimen was 12.04 ± 1.42% (SEM). It was not correlated with the BTS (–0.222; P = 0.3017) nor with the density of NFT (r = –0.073; P = 0.74). Taking the shrinkage into account in the estimate of the density of the neuronal profiles only slightly altered the correlations (correlations between the density of neuronal profiles and BTS: 0.40; P < 0.04; between the density of neuronal profiles and NFT: –0.52; P < 0.005).

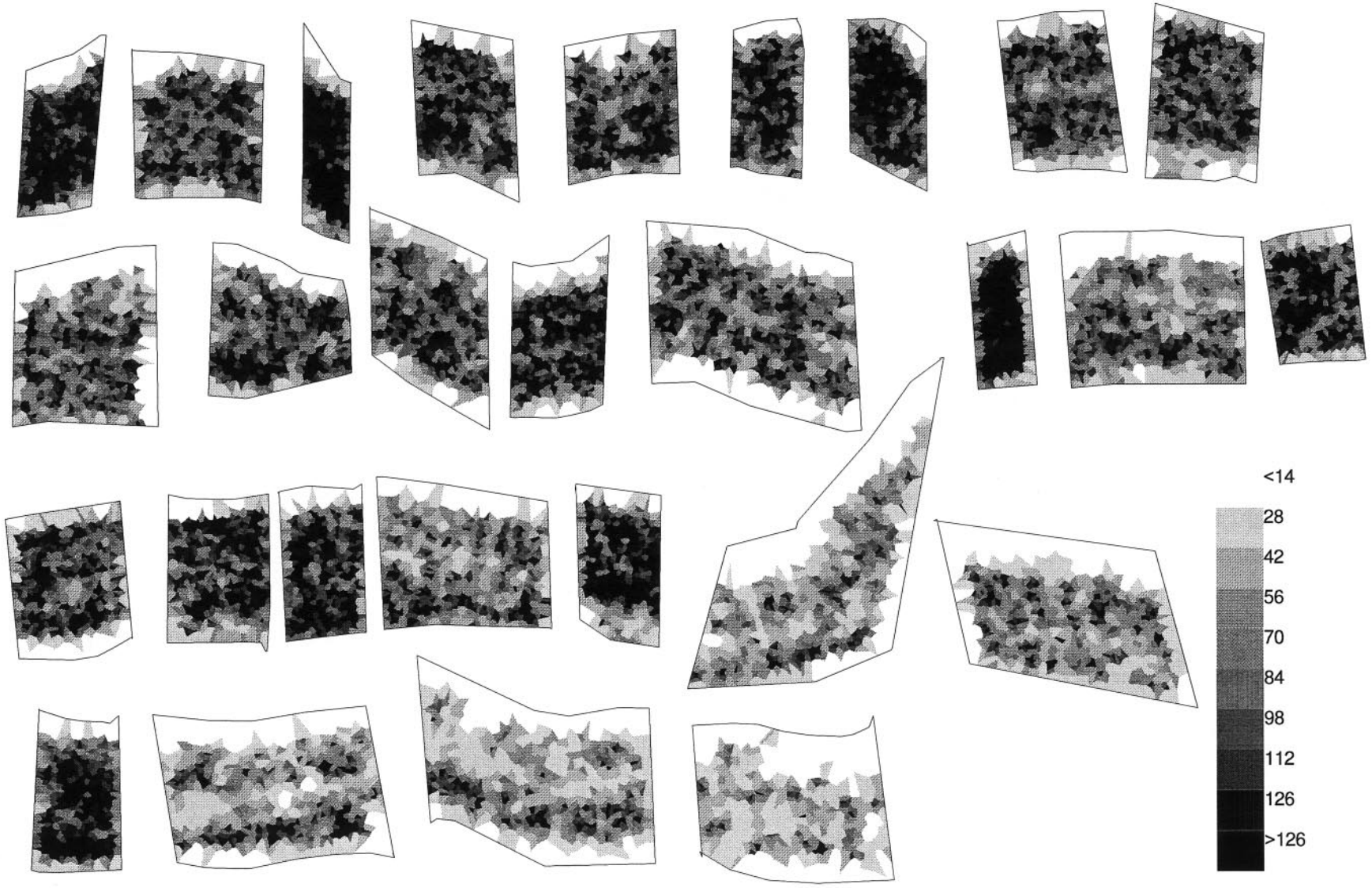

Fig. 4 Density map after standardization of the cortical thickness. Same maps as in Fig. 2. The cortical thickness was standardized to 3000 μm. Each map was dilated or contracted in such a way that the thickness reached this value. The samples are ranked in the same order as in Fig. 2 according to NFT density and BTS (least affected case, *top left*; most affected one, *bottom right*). Densities are in number of profiles per mm^2. The standardization made the neuronal loss more readily apparent than in Fig. 2

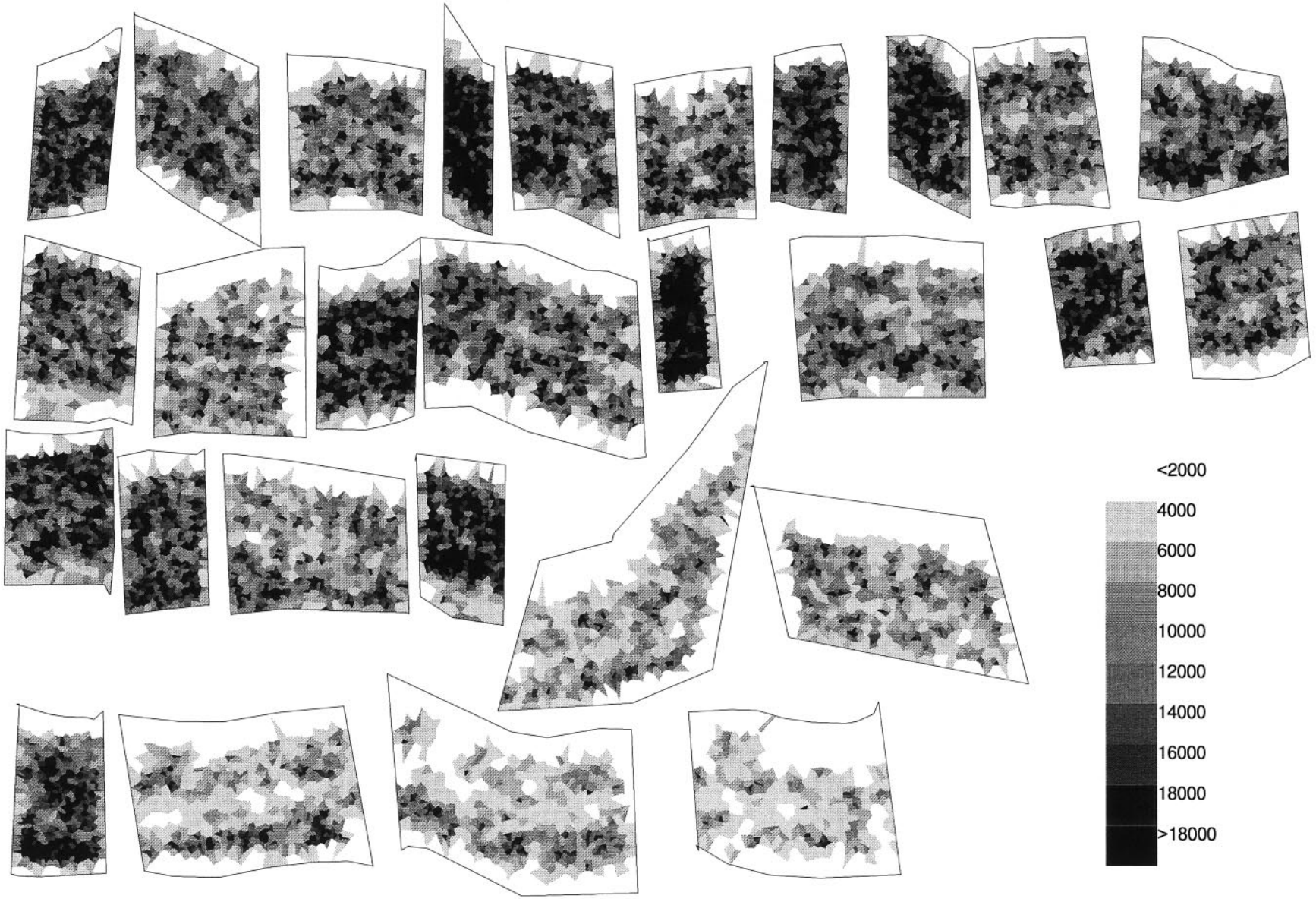

Fig. 5 Density map of the number of neurons per mm^3; same map as in Fig. 4. Cases were ranked as previously: normal case, *top left*; most affected case: *bottom right*. Number of neurons per unit volume, *Nv*, was calculated from Abercrombie formula [1], taking into account the thickness of the section which was measured for each sample and the diameter of the nucleolus (2.839 μm). The density was also corrected for the shrinkage of the block

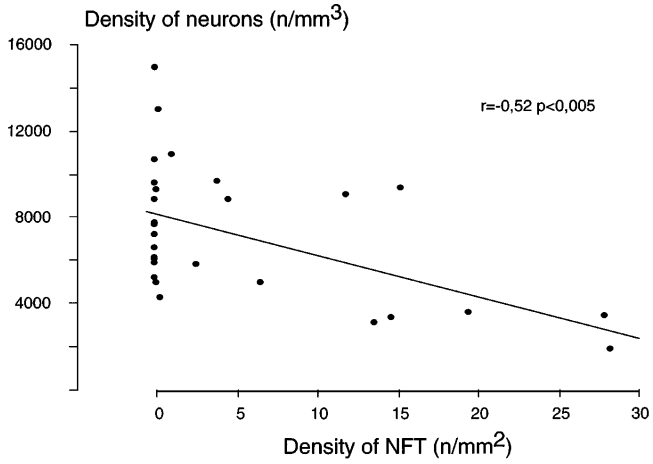

Fig. 6 Regression of the density of neurons (number/mm^3) on the density of NFT profiles (number/mm^2). The density of neurons was statistically linked with the density of NFT, although the relationship appeared to be loose and to suffer several exceptions: notice the large dispersion in the density values for the cases with no NFT. The statistical relationship mainly depended on the most affected cases, in which the density of neurons was very low

Estimation of the density of neurons per mm^3

The neuronal density appeared to be decreased in the most affected case (Fig. 5). The neuronal density was on average 7157 ± 612 neurons/mm^3 and was correlated with the BTS (r = 0.40; P < 0.04) and with the density of the NFT (r = –0.52; P < 0.005), as illustrated in Fig. 6.

Laminar topography of the neuronal loss

The cortex, thickness of which had been standardized at 3000 μm, was divided into ten bands, parallel to the pial surface. A correlation between the density of the neurons in each band and the density of the NFT was sought. The statistical significances of these coefficients are shown in Fig. 7, in connection with the layer probability (from [13]). Two peaks were observed: one was situated in the superficial region of layer III. The layer corresponding to the second peak was more difficult to localize, being situated at mid-distance between the pial surface and the white matter, most probably in the deepest part of layer III.

Relationship between the neuronal density and the density of NFT

The relationship between the neuronal density and the density of NFT appeared to be loose and to suffer many exceptions as seen in Fig. 6. The high value of the correlation coefficient seemed to be mainly related to the very low neuronal densities observed in a few cases which exhibited the largest number of NFT. When the two cases with the highest values of NFT density were dropped, the correlation failed to reach significance. The threshold in

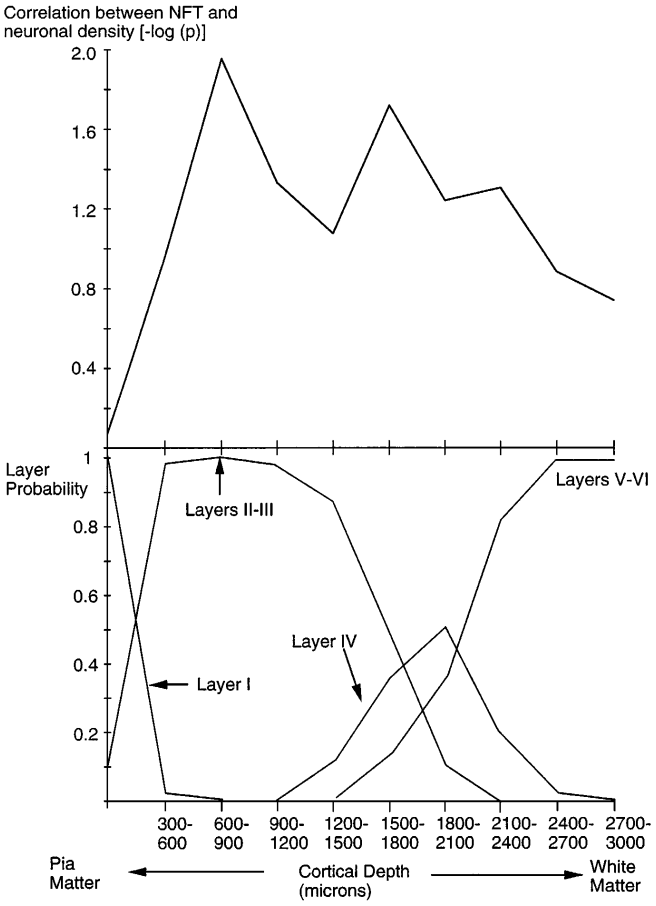

Fig. 7 Correlation between the neuronal density and the density of the NFT. The abscissa represents the cortical depth on a standardized scale of 3000 μm. The mean density of neurons has been calculated in each sample (1 per case; 28 cases) in ten bands (100 μm in height), parallel to the pial surface. The *upper view* shows the correlation between the neuronal density in each of the ten bands and the mean density of NFT profiles. The coefficient r of Pearson correlation between these two values has been calculated in the whole population for each band. To take into account the distribution of sample correlation coefficients, the P values (rather than the coefficients themselves) were tabulated. Log_{10} were taken to cover more easily the whole range of values. To avoid negative values -log(P) is shown. The lower view is the layer probability as a function of cortical depth (from [13]). The best correlation was reached at depth 600–900 μm from the pial surface, i.e., in layer II, upper part of layer III

the density of NFT that made the largest difference in neuronal density between two groups was found to be 5 NFT/mm^2: the group with fewer than 5 NFT/mm^2 comprised 20 cases; the mean neuronal density was 9151 ± 683 neurons/mm^3. The group with more than 5 NFT/mm^2 comprised 8 cases with a mean (standardized) neuronal density of 5475 ± 1192 neurons/mm^3. The mean difference between the two groups was 3677 neurons/mm^3 (P < 0.01), i.e., a mean loss of 40%. The morphometric characteristics of the two groups are shown in Table 1.

Table 1 Comparison of the cases with more than 5 neurofibrillary tangles/mm^2 with the rest of the population. *n* Number, *NFT* = neurofibrillary tangles, *BTS* = Blessed test score. Differences in neuronal densities were significant only when the thickness of the cortex was standardized. This is due to the masking of the neuronal loss by the cortical atrophy. The total number of neurons (taking into account the volume of the lobe) was much lower in the group with more than 5 NFT/mm^2

	≤ 5 NFT/mm^2	> 5 NFT/mm^2
n	20	8
BTS	17.6 ± 1.89	2.8 ± 0.72***
Mean density of neuronal profiles	102 ± 4.9	91.5 ± 7.0 (NS)
Mean density of neuronal profiles (thickness standardized at 3000 μm)	89 ± 5.9	56 ± 11.4**
Mean neuronal density (*n*/mm^3)	9029 ± 416.6	7496 ± 697.6 (NS)
Mean neuronal density (*n*/mm^3) (thickness standardized at 3000 μm)	9151.5 ± 683.4	5475 ± 1192.5**
Volume of the parietal lobe	35 ± 1.7	27 ± 2.2*
Total number	(313 ± 16) × 10^6	(215 ± 30) × 10^6***

**** $P < 0.0001$; *** $P < 0.005$; ** $P < 0.01$; * $P < 0.02$

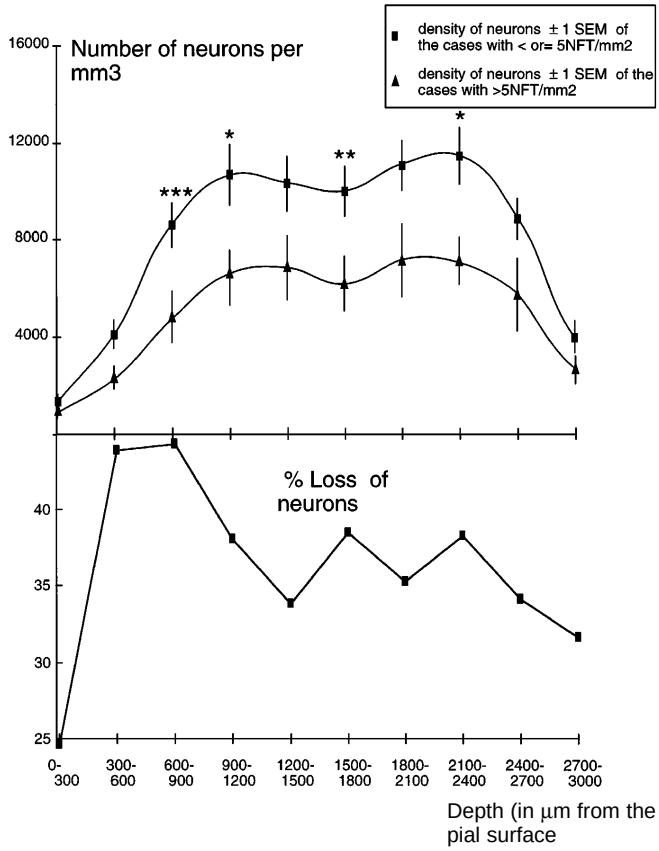

Fig. 8 Neuronal densities in the cases with fewer than 5 NFT/mm^2 compared to those with more. *Upper view*: neuronal density of the population with less than 5 NFT profiles/mm^2 (*n* = 20; *upper curve*) and the population with more than 5 NFT profiles per mm^2 (*n* = 8; *lower curve*). Results are expressed in number of neurons per mm^3 ± SEM. The lines between the experimental points were interpolated. *** $P < 0.01$; ** $P < 0.03$; * $P < 0.05$. The difference was most significant at depth 600–900 μm (layer II; *upper part* of layer III). *Lower view*: the curve represents the percent loss of neurons: (difference between the experimental points of the *upper view* × 100)/density of neurons in the cases with fewer than 5 NFT/mm^2. The maximal value was reached at 600–900 μm

Laminar neuronal loss

The difference in neuronal density between the two groups was calculated within ten bands parallel to the pial surface (Fig. 8). Significant differences were found for values of cortical thickness of 600–900 μm, 900–1200 μm, 1500–1800 μm and 2100–2400 μm. The correlations were already found to be the most significant at depths 600–900 μm and 1500–1800 μm. The mean loss in the upper part of layer III reached 4123 neurons/mm^3, i.e., 44% of the value observed in the cases with fewer than 5 NFT/mm^2. The loss at 1500–1800 μm of depth was 4201 neurons/mm^3 (37%) and at 2100–2400 μm 4771 neurons/mm^3 (37%).

Total number of neurons: relationship with the density of NFT in the parietal lobe

The volume of the parietal lobe (mean 33.2 cm^3) was correlated with the NFT density ($r = -0.503$; $P < 0.006$). The rough estimate of the total number of neurons yielded a mean value of $285 \times 10^6 \pm 16 \times 10^6$. The correlation between the total number of neurons and the density of NFT was significant ($r = -0.634$ $P < 0.004$). The following equation described the regression line: total number of neurons = 319×10^6 neurons $-6 \times 10^6 \times$ density of NFT (/mm^2), indicating that 1 tangle/mm^2 seen on the slide corresponded, on average, to a loss of 6×10^6 neurons in the parietal lobe. The difference between the number of neurons in the cases with fewer than 5 NFT/mm^2 ($313 \times 10^6 \pm 16 \times 10^6$) compared to those with more than that value ($215 \times 10^6 \pm 30 \times 10^6$) reached 98×10^6 ($t = 3.167$; $P < 0.005$), i.e., 31%.

Most significant alteration in regard to dementia

To test the relative importance of the neuronal loss and of the NFT in the correlation to dementia, a step by step mul-

tiple regression, involving the intellectual status (BTS) as the dependent variable and the density of NFT and of neurons as the independent variables indicated that the best correlate was the density of NFT. Once taken into account, the total number of neurons was found to have too little significance to be also included in the model.

Discussion

We mapped the neurons in a sample from the supramarginal gyrus of the parietal lobe in a cohort of prospectively assessed individuals, either intellectually normal or affected by AD of varying severity. The supramarginal gyrus is an associative multimodal cortex, vulnerable to neurofibrillary pathology [3] at Braaks' stage VI when cognitive deficits become apparent in other functions than memory. It is spared in the least affected cases of this series and severely involved in the most affected ones [20]. The densities of the NFT, SP and Aβ deposits were also available in the same samples [10, 11, 13]. The volume of the parietal lobe, the shrinkage of the histological sample, the section thickness were assessed and taken into account. The new method that we have used to measure the neuronal density allows a laminar analysis of the loss. We found that it was maximal at the upper part of layers II–III and was mainly correlated with the density of NFT. It reached significant values only in the group of patients with a density of NFT higher that 5 NFT/mm^2, where it amounted to an approximate loss of 98×10^6 neurons when extrapolated to the entire parietal lobe.

Atrophy and density

Although still a matter of debate [23, 42], some neuronal loss has been found in most studies dealing with the isocortex [23, 32, 37–40, 45, 47]. All the positive results have been obtained after having taken the atrophy into account, mostly by standardizing the cortical thickness. Whatever the procedure, it tends to lower the neuronal density of atrophic cortex by artificially stretching the cortical ribbon. However, since the cortical thickness itself is correlated with the density of NFT, the standardization might artificially add some significance to results which would have otherwise remained negative.

On the other hand, as already stressed [18, 28], the loss of neurons in the cortex does not leave "holes" that would induce a drop in cellular density, but causes atrophy. Atrophy, in turn, tends to restore a normal neuronal density and to mask the loss [7]. To unmask this, two procedures were used alternatively in this study: the data were corrected to obtain a standardized cortical thickness and a macroscopic measure of the volume of the parietal lobe was performed.

Sample shrinkage and section thickness

To the best of our knowledge, the shrinkage due to the paraffin embedding has never been measured in studies dealing with AD, although it has been shown to be influenced by age [27]. We have measured the section thickness for each slide. Much to our surprise, this value appeared to be variable and to have some positive correlation with the density of the NFT.

Control of the stereological bias

Large neurons have a higher probability of being cut than small ones, so that their profiles are overrepresented on a microscopical section. Shrinkage of neuronal perikarya decreases the density of the corresponding neuronal profiles [46], a decrease that remains lower than the corresponding increase in the density of the smaller profiles [16]. The best way, at least theoretically, of avoiding this "pseudo-loss" is to use the disector [43], but the constraints of that technique make the mapping of the neurons difficult. To determine the bias, we counted small structures (nucleoli, exhibiting an average diameter of 2.84 μm) relative to the section thickness (7 μm). Although nucleolar atrophy was not substantiated in this series of cases, it has been reported to occur during the course of AD. The maximal values of the reduction in the nucleolar volume in the isocortex, reported by Mann et al. [38], was 56%; this corresponds to a radius of 0.76 times the control value (cubic root of 1–0.56). A reduction of 24% of the diameter of the nucleolus would account at the most for a bias of less than 6% (see chart in [16]), a value that was found to be much smaller than the experimental error and, therefore, of an acceptable magnitude in regard to the information gained in mapping the topography of the neurons.

We, thus, concluded that the decrease in the density of the neuronal profiles, with the method that we used and the corrections that we applied, was a consequence of a neuronal loss and not an artifact.

Most severely affected layers

The neuronal loss involved all layers as illustrated by the maps in Fig. 8. However, it was of unequal magnitude. The maximal loss reached 45% in layer II and upper part of layers III, with minimal values being observed in the depth of the cortex. The selectivity of the neuronal loss for the upper layers might be compared to that seen in the entorhinal cortex: layer II neurons, also located in the upper part of the cortex, stand the brunt of the pathology [22]. The selective vulnerability of these neurons is presently poorly understood and may be explained in various ways. The connections could be of importance since these neurons are mainly involved in corticocortical relations [9, 13, 17, 31–34, 36, 41, 48]. Vascular factors are not known to affect the superficially located neurons predominantly and we are not aware of a neurotransmitter that would be specific for those cells, which might, however, be defined by some subtypes of neurofilament [31].

Total number of neurons

Although a gross estimate of the neuronal loss, the value that was provided here shows that the neuronal destruction may be of a much larger magnitude than believed in the view of the (relatively) small decrease in the neuronal density and emphasizes the necessity of assessing the volume of the cortex. Atrophy indeed appears to be a more reliable index of neuronal loss in the cortex than the decrease in neuronal density. Our estimates are at variance with the results of Regeur et al. [42] who studied the total number of cortical neurons and found no significant difference between a demented and a control population. They are, however, in good agreement with other recent studies [22, 23] showing the severity and the selectivity of the neuronal loss.

Relationship between NFT and neuronal loss: connection with the intellectual deficit

The NFT were the only pathological lesions that were strongly correlated with the neuronal loss. It should also be noticed that the major neuronal loss occurred in those layers where NFT are known to be most numerous [10, 36]. Finally, it can be stressed that the loss was detectable only in those cases where the NFT density was over the threshold of 5 profiles/mm^2.

Our method of counting NFT prevented any attempt of evaluating their total number. A previous study, however, underlined the excess of neuronal loss in the isocortex when compared to the number of NFT [23] and suggested that "the majority of neuronal loss in advanced AD occurs through a non-NFT mechanism". The proportion of NFT to neuronal loss in this study (6×10^6 neurons in the parietal lobe for 1 NFT/mm^2) is in agreement with this statement as is the low density of extracellular tangles in the isocortex. In the hippocampus, where extracellular tangles accumulate, a good correlation between neuronal loss and tangle formation has been found [8]. A correlation between SP and neuronal loss has been reported [21], albeit in a very old population (older than 96 years) in which there was no link between tangle and neuron densities. This may be partly explained by the lower severity of the changes in people of advanced age [26], but the possible uncoupling between neuronal loss and tangle formation may also suggest that, at least in the isocortex, they are correlated because of contemporary occurrence rather than because of a causal relationship. In an attempt to find the best correlate of the intellectual deficit, we determined, in a step by step analysis, that this was represented by the NFT density rather than the neuronal loss. Since NFT density and neuronal number were themselves correlated, neuronal number lost all explanatory value when the NFT were introduced in the model. NFT might, thus, be a more direct cause of the intellectual deficit than neuronal death, which probably represents a late stage in the cascade of events taking place in the disease.

Conclusion

We have shown that a severe neuronal loss occurred in area 40 during the latest stages of AD. The severity of this loss could be assessed only if the atrophy of the cortex was taken into account. The loss was correlated with, although not necessarily caused by, the presence of NFT. A threshold of 5 NFT/mm^2 appeared to distinguish the group with neuronal loss from that without, although large variations were observed in individual values. The loss seemed to be, at least partially, layer specific and to involve mainly neurons located in layers II and upper part of layer III, said to be involved in corticocortical connections.

Acknowledgements We gratefully acknowledge the expertise of Prof. F. Piette who collected the clinical data. This work has been supported by Association Claude Bernard.

References

1. Abercrombie M (1946) Estimation of nuclear populations from microtome sections. Anat Rec 94:239–247
2. Arnold SE, Hyman BT, Flory J, Damasio AR, Van Hoesen GW (1991) The topographical and neuroanatomical distribution of neurofibrillary tangles and neuritic plaques in the cerebral cortex of patients with Alzheimer's disease. Cereb Cortex 1:103–116
3. Arnold SE, Hyman BT, Van Hoesen GW (1994) Neuropathologic changes of the temporal pole in Alzheimer's disease and Pick's disease. Arch Neurol 51:145–150
4. Billingsley PR, Ranson SW (1918) On the number of nerve cells in the ganglion cervicale superius and of nerve fibers in the cephalic end of the truncus sympathicus in the cat and on the numerical relations of preganglionic and postganglionic neurons. J Comp Neurol 29:359–366
5. Braak H, Braak E (1991) Neuropathological stageing of Alzheimer-related changes. Acta Neuropathol 82:239–259
6. Brun A, Englund E (1981) Regional pattern of degeneration in Alzheimer's disease: neuronal loss and histopathological grading. Histopathology 5:549–564
7. Coleman PD, Flood DG (1987) Neuron numbers and dendritic extent in normal aging and Alzheimer's disease. Neurobiol Aging 8:521–545
8. Cras P, Smith MA, Richey PL, Siedlak SL, Mulvihill P, Perry G (1995) Extracellular neurofibrillary tangles reflect neuronal loss and provide further evidence of extensive protein cross-linking in Alzheimer disease. Acta Neuropathol 89:291–295
9. Delacoste MC, White CL (1993) The role of connectivity in Alzheimer's disease pathogenesis. A review and model system. Neurobiol Aging 14:1–16
10. Delaère P, Duyckaerts C, Brion JP, Poulain V, Hauw J-J (1989) Tau, paired helical filaments and amyloid in the neocortex: a morphometric study of 15 cases with graded intellectual status in aging and senile dementia of Alzheimer type. Acta Neuropathol 77:645–653
11. Delaère P, Duyckaerts C, He Y, Piette F, Hauw J-J (1991) Subtypes and differential laminar distributions of βA4 deposits in Alzheimer's disease: relationship with the intellectual status of 26 cases. Acta Neuropathol 81:328–335
12. Duyckaerts C, Hauw J-J, Piette F, Rainsard C, Poulain V, Berthaux P, Escourolle R (1985) Cortical atrophy in senile dementia of the Alzheimer type is mainly due to a decrease in cortical length. Acta Neuropathol (Berl) 66:72–74
13. Duyckaerts C, Hauw J-J, Bastenaire F, Piette F, Poulain C, Rainsard V, Javoy-Agid F, Berthaux P (1986) Laminar distribution of neocortical plaques in senile dementia of the Alzheimer type. Acta Neuropathol (Berl) 70:249–256

14. Duyckaerts C, Brion J-P, Hauw J-J, Flament-Durand J (1987) Quantitative assessment of the density of neurofibrillary tangles and senile plaques in senile dementia of the Alzheimer type. Comparison of immunocytochemistry with a specific antibody and Bodian's protargol method. Acta Neuropathol (Berl) 73:167–170
15. Duyckaerts C, Kawasaki H, Delaère P, Rainsard C, Hauw J-J (1989) Fiber disorganization in the neocortex of patients with senile dementia of the Alzheimer type. Neuropathol Appl Neurobiol 15:233–247
16. Duyckaerts C, Llamas E, Delaère P, Miele P, Hauw J-J (1989) Neuronal loss and neuronal atrophy. Computer simulation in connection with Alzheimer's disease. Brain Res 504:94–100
17. Duyckaerts C, Delaère P, Hauw JJ (1992) Alzheimer's disease and neuroanatomy: hypotheses and proposals. In: Boller F, Forette F, Khachaturian Z, Poncet M, Christen Y (eds) Heterogeneity of Alzheimer's disease. Springer, Berlin Heidelberg New York, pp 144–155
18. Duyckaerts C, Delaère P, Costa C, Hauw J-J (1993) Factors influencing neuronal density on sections: quantitative data obtained by computer simulation. In: Computers and computations in the neurosciences. Academic Press, San Diego, pp 526–548
19. Duyckaerts C, Godefroy G, Hauw J-J (1994) Evaluation of neuronal numerical density by Dirichlet tessellation. J Neurosci Methods 51:47–69
20. Duyckaerts C, Bennecib M, Grignon Y, Uchihara T, He Y, Piette F, Hauw J-J (1997) Modeling the relation between neurofibrillary tangles and intellectual status. Neurobiol Aging 18:267–273
21. Giannakopoulos P, Hof PR, Kovari E, Vallet PG, Herrmann FR, Bouras C (1996) Distinct pattern of neuronal loss and Alzheimer's disease lesion distribution in elderly individuals older than 90 years. J Neuropathol Exp Neurol 55:1210–1220
22. Gomez-Isla T, Price JL, McKeel DW Jr, Morris JC, Growdon JH, Hyman BT (1996) Profound loss of layer II entorhinal cortex neurons occurs in very mild Alzheimer's disease. J Neurosci 16:4491–4500
23. Gomez-Isla T, Hollister R, West H, Mui S, Growdon JH, Petersen RC, Parisi JE, Hyman BT (1997) Neuronal loss correlates with but exceeds neurofibrillary tangles in Alzheimer's disease. Ann Neurol 41:17–24
24. Gundersen HJG, Jensen EB (1987) The efficiency of systematic sampling in stereology and its prediction. J Microsc 147:229–263
25. Gundersen HJG, Bagger P, Bendtsen TF, Evans SM, Korbo L, Marcussen N, Moller A, Nielsen K, Nyengaard JR, Pakkenberg B, Sorensen FB, Verserby A, West MJ (1988) The new stereological tools: disector, fractionator and point sampled intercepts and their use in pathological research and diagnosis. Acta Pathol Microbiol Immunol Scand 96:857–881
26. Hansen LA, DeTeresa R, Davies P, Terry RD (1988) Neocortical morphometry, lesion counts, and choline acetyltransferase levels in the age spectrum of Alzheimer's disease. Neurology 38:48–54
27. Haug H (1980) Die Abhängigkeit der Einbettungsschrumpfung des Gehirngewebes vom Lebensalter. Verh Anat Ges 74:699–700
28. Hauw JJ, Duyckaerts C, Partridge M (1986) Neuropathological aspects of brain aging and SDAT. In: Courtois YA (ed) Modern trends in aging research. Inserm-Eurage/John Libbey Eurotext, London, pp 435–442
29. He Y, Delaère P, Duyckaerts C, Wasowicz M, Piette F, Hauw JJ (1993) Two distinct ubiquitine immunoreactive senile plaques in Alzheimer's disease: relationship with the intellectual status in 29 cases. Acta Neuropathol 86:109–116
30. He Y, Duyckaerts C, Delaère P, Piette F, Hauw J-J (1993) Alzheimer's lesions labelled by anti-ubiquitin antibodies. Comparison with other staining techniques. Neuropathol Appl Neurobiol 19:364–371
31. Hof PR, Nimchinsky EA, Morrison JH (1995) Neurochemical phenotype of corticocortical connections in the Macaque monkey: quantitative analysis of a subset of neurofilament protein-immunoreactive projection neurons in frontal, parietal, temporal, and cingulate cortices. J Comp Neurol 362:109–133
32. Hyman TB, Gomez-Isla T (1994) Alzheimer's disease is a laminar, regional, and neural system specific disease, not a global brain disease. Neurobiol Aging 15:353–354
33. Hyman BT, Hoesen GWV, Damasio AR, Barnes CL (1984) Alzheimer's disease: cell-specific pathology isolates the hippocampal formation. Science 225:1168–1170
34. Hyman BT, Duyckaerts CD, Christen Y (1997) Connections, cognition and Alzheimer disease. Springer, Berlin Heidelberg New York
35. Kino KS (1990) Intermediate optics in Nipkow disk microscopes. In: Pawley JB (ed) Handbook of biological confocal microscopy. Plenum Press, New York, p 108
36. Lewis DA, Campbell MJ, Terry RD, Morrison JH (1987) Laminar and regional distribution of neurofibrillary tangles and neuritic plaques in Alzheimer's disease. A quantitative study of visual and auditory cortices. J Neurosci 7:1799–1808
37. Mann DMA (1994) Pathological correlates of dementia in Alzheimer's disease. Neurobiol Aging 15:357–360
38. Mann DMA, Yates PO, Marcyniuk B (1985) Some morphometric observations on the cerebral cortex and hippocampus in presenile Alzheimer's disease, senile dementia of Alzheimer type and Down's syndrome in middle age. J Neurol Sci 69:139–159
39. Mann DMA, Marcyniuk B, Yates PO, Neary D, Snowden JS (1988) The progression of the pathological changes of Alzheimer's disease in frontal and temporal neocortex examined both at biopsy and at autopsy. Neuropathol Appl Neurobiol 14:177–195
40. Mountjoy CQ, Roth M, Evans NJR, Evans HM (1983) Cortical neuronal counts in normal elderly controls and demented patients. Neurobiol Aging 4:1–11
41. Pearson RCA, Esiri MM, Hiorns RW, Wilcock GK, Powell TPS (1985) Anatomical correlates of the distribution of the pathological changes in the neocortex in Alzheimer disease. Proc Natl Acad Sci USA 82: 4531–4534
42. Regeur L, Badsberg Jensen G, Pakkenberg H, Evans SM, Pakkenberg B (1994) No global neocortical nerve cell loss in brains from patients with senile dementia of Alzheimer's type. Neurobiol Aging 15:347–352
43. Sterio DC (1984) The unbiased estimation of number and sizes of arbitrary particles using the disector. J Microsc 134:127–136
44. Terry RD, Fitzgerald C, Peck A, Millner J, Farmer P (1977) Cortical cell counts in senile dementia. J Neuropathol Exp Neurol 36:633
45. Terry RD, Peck A, DeTeresa R, Schechter R (1981) Some morphometric aspects of the brain in senile dementia of the Alzheimer type. Ann Neurol 10:184–192
46. Terry RD, DeTeresa R, Hansen LA (1987) Neocortical cell counts in normal human adult aging. Ann Neurol 21:530–539
47. Terry RD, Masliah E, Salmen DP, Butters N, DeTeresa R, Hill R, Hansen LA, Katzman R (1991) Physical basis of cognitive alterations in Alzheimer's disease: synapse loss is the major correlate of cognitive impairment. Ann Neurol 30:572–580
48. Van Hoesen GW (1997) Cortical feedforward and cortical feedback neural systems in Alzheimer's disease. In: Hyman BT, Duyckaerts C, Christen Y (eds) Connections, cognition and Alzheimer's disease. Springer, Berlin Heidelberg New York, pp 17–31
49. Weibel ER (1979) Stereological methods. Practical methods for biological morphometry. Academic Press, London, p 53
50. West MJ, Coleman PD, Flood DG, Troncoso JC (1994) Differences in the pattern of hippocampal neuronal loss in normal aging and Alzheimer disease. Lancet 344:769–772